Received: 17 March 2021 | Accepted: 12 May 2021

DOI: 10.1002/htj.22192

RESEARCH ARTICLE

HEAT TRANSFER WILEY

Three-dimensional hydromagnetic hybrid nanoliquid flow and heat transfer between two vertical porous plates moving in opposite directions: Sensitivity analysis

Alphonsa Mathew | **T. S. Neethu** | **Sujesh Areekara**

Department of Mathematics, St. Thomas' College (Autonomous), Thrissur, Kerala, India

Correspondence
Alphonsa Mathew, Department of Mathematics, St. Thomas' College (Autonomous), Thrissur, Kerala 680001, India.
Email: alphonsa@stthomas.ac.in

Abstract

The hydromagnetic convective flow between two parallel plates has been analyzed frequently. However, only a countable number of studies are accounted for the flow between parallel plates moving in opposite directions. The present work aims to analytically explore the three-dimensional (3D) convective hydromagnetic hybrid nanoliquid (with suspended Al_2O_3 and Fe_3O_4 nanoparticles) flow between two oppositely moving vertical porous plates utilizing the perturbation technique. The consequence of effectual parameters on the flow profiles is analyzed with the aid of graphs using MATLAB software. It is perceived that nanoparticle volume fraction ascends drag coefficient and descends temperature and main flow velocity. Furthermore, the rate of heat transfer is statistically scrutinized utilizing response surface methodology and sensitivity analysis. It is noted that the Nusselt number is most sensitive with the injection parameter. 3D surface plots are used to illustrate the parallel effect of pertinent parameters on the drag coefficient. Moreover, the present study finds applications in several engineering, geophysical, and industrial fields, such as in heat exchangers and faulting.

KEYWORDS

hybrid nanoliquid, magnetohydrodynamics, opposite moving plates, porous plate, response surface methodology, sensitivity analysis

1 | INTRODUCTION

The latest nanotechnology research works focus on finding practices that help in boosting the efficiency and transfer properties of the considered nanoliquid (fluids suspended with nanoparticles). This is where hybrid nanoliquid (colloidal suspension of two or more nanomaterials) comes into the scene. The collaborative effect alters the nanoliquid's heat transfer rate proving to be beneficial in many engineering and industrial fields (like solar energy systems, car radiators, nuclear system cooling, micromanufacturing processes, etc.). Junoh et al.[1] numerically explored the consequence of induced magnetic field (IMF) on the heat transfer and hydromagnetic stagnation point flow over a lengthening/shortening sheet and revealed that the heat transfer rate was higher for the hybrid nanoliquid. Acharya and Mabood[2] employed the fourth-order Runge–Kutta method to numerically inspect the hybrid nanoliquid flow over a slippery permeable bent structure. They perceived that the hybrid nanoliquid exhibits a lower drag coefficient and higher Nusselt number. Some recent studies concerning hybrid nanoliquid can be seen in References [3–6].

Employment of magnetic fields assures prospective significance in the field of geophysics, industrial engineering, and biomedical fields. Jha and Aina[7] theoretically explored the influence of IMF on free convective flow in a vertical microchannel and reported that augmenting magnetic Prandtl number and Hartmann number causes a decrease in volume flow rate. Dash and Ojha[8] discussed the MHD viscoelastic fluid flow between two infinite horizontal permeable plates involving sinusoidal pressure gradient and noted a decline in velocity profile on amplifying Hartmann number. A few studies reporting the consequence of magnetic field can be seen in References [9–12].

A porous plate corresponds with a plate having frequently distributed void spaces in it. They are found to be beneficial in oil reservoirs, agricultural engineering, petroleum technology, and so forth. Nayak et al.[13] numerically analyzed the three-dimensional (3D) hydromagnetic nanoliquid flow through an exponentially lengthening porous sheet with the aid of the fourth-order Runge–Kutta method. They noticed a rise in velocity with augmenting porosity parameter values. Das et al.[14] inspected the impact of the transverse magnetic field, slip condition, and Hall current on an unsteady hydromagnetic rotating flow over a periodically accelerated horizontal porous plate. They noted that increasing Hall current has a positive effect on the velocity profile close to the plate and a negative effect on the velocity profile away from the plate. Studies dealing with porous plates considering different attributes are explained in References [15–19].

Analysis of physical quantities (heat transfer rate/drag coefficient/mass transfer rate) utilizing statistical techniques (like correlation, regression, sensitivity analysis) has recently trended in the research world due to its efficiency in producing accurate quantitative results. response surface methodology (RSM) analyzes the conjoint impact of effectual parameters (independent variables) on the physical quantity of interest (response/dependent variable). Sensitivity analysis, on the other hand, measures the extent and nature of dependency exhibited by the effectual parameters on the physical quantity of interest. Some recent explorations on RSM and sensitivity analysis can be viewed in References [20–23].

Even though many investigations concerning hydromagnetic convective flow between two parallel plates have been carried out, only a handful of studies discusses the flow between parallel plates moving in different directions.[24–27] Neethu et al.[28] analytically inspected the 3D hydromagnetic nanoliquid flow between two vertical porous plates moving in different directions with the aid of the perturbation technique. They perceived that injection parameter enhances the temperature profile whereas nanoparticle volume fraction diminishes the temperature profile.

Impelled by previous studies, it is heeded that 3D hydromagnetic hybrid nanoliquid flow of hybrid nanoliquid between two vertical porous plates moving in opposite directions has not yet been explored. The current work aims at filling this gap. The present study finds applications in several engineering, geophysical, and industrial fields like heat exchangers and faulting. Moreover, sensitivity analysis on the rate of heat transfer is also incorporated to boost the novelty of the present work.

2 | PROBLEM STATEMENT

An unsteady convective hybrid nanoliquid flow between two vertical porous plates involving a magnetic field (of uniform strength, B_0 applied normal to the plane of the plate) is considered (see Figure 1). The problem is developed utilizing the following conditions:

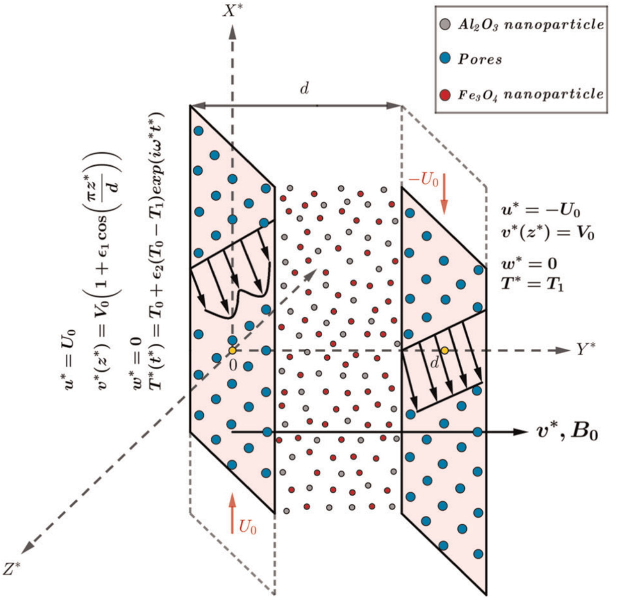

FIGURE 1 Physical configuration [Color figure can be viewed at wileyonlinelibrary.com]

(i) Parallel plates are traveling in different directions with uniform velocity.
(ii) The upward and downward-moving plates are subjected to transverse sinusoidal injection velocity and constant suction velocity, respectively.
(iii) An IMF has been neglected due to the assumption of a small magnetic Reynolds number.
(iv) The injection velocity distribution is of the form:

$$v^*(z^*) = V_0\left(1 + \varepsilon_1 \cos\left(\frac{\pi z^*}{d}\right)\right).$$

(v) Without loss of generality, the distance d between the plates is taken equal to the wavelength of the injection velocity.
(vi) The temperature of the downward-moving plate is at constant temperature T_1 and that of the upward-moving plate fluctuating with time is given as:

$$T^*(t^*) = T_0 + \varepsilon_2(T_0 - T_1)e^{i\omega^* t^*}.$$

Utilizing Boussinesq's approximation and the above assumptions, governing equations are given by[24,28]:

$$\frac{\partial v^*}{\partial y^*} + \frac{\partial w^*}{\partial z^*} = 0, \tag{1}$$

$$\frac{\partial u^*}{\partial t^*} + v^*\frac{\partial u^*}{\partial y^*} + w^*\frac{\partial u^*}{\partial z^*} = -\frac{1}{\rho_{hnf}}\left[\frac{\partial p^*}{\partial x^*} - \mu_{hnf}\left(\frac{\partial^2 u^*}{\partial y^{*2}} + \frac{\partial^2 u^*}{\partial z^{*2}}\right) + \sigma_{hnf} B_0^2 u^*\right] + g\beta_{hnf}(T^* - T_1), \tag{2}$$

$$\frac{\partial v^*}{\partial t^*} + v^*\frac{\partial v^*}{\partial y^*} + w^*\frac{\partial v^*}{\partial z^*} = -\frac{1}{\rho_{hnf}}\left[\frac{\partial p^*}{\partial y^*} - \mu_{hnf}\left(\frac{\partial^2 v^*}{\partial y^{*2}} + \frac{\partial^2 v^*}{\partial z^{*2}}\right)\right], \tag{3}$$

$$\frac{\partial w^*}{\partial t^*} + v^*\frac{\partial w^*}{\partial y^*} + w^*\frac{\partial w^*}{\partial z^*} = -\frac{1}{\rho_{hnf}}\left[\frac{\partial p^*}{\partial z^*} - \mu_{hnf}\left(\frac{\partial^2 w^*}{\partial y^{*2}} + \frac{\partial^2 w^*}{\partial z^{*2}}\right) + \sigma_{hnf} B_0^2 w^*\right], \tag{4}$$

$$\frac{\partial T^*}{\partial t^*} + v^*\frac{\partial T^*}{\partial y^*} + w^*\frac{\partial T^*}{\partial z^*} = \frac{k_{hnf}}{(\rho c_p)_{hnf}}\left[\frac{\partial^2 T^*}{\partial y^{*2}} + \frac{\partial^2 T^*}{\partial z^{*2}}\right], \tag{5}$$

subject to the boundary conditions:

$$\left.\begin{aligned} y^* = 0,\ \ u^* = U_0,\ \ v^*(z^*) = V_0\left(1 + \varepsilon_1 \cos\frac{\pi z^*}{d}\right), \\ w^* = 0,\ \ T^*(t^*) = T_0 + \varepsilon_2(T_0 - T_1)e^{i\omega^* t^*}, \\ y^* = d,\ \ u^* = -U_0,\ \ v^*(z^*) = V_0,\ \ w^* = 0,\ \ T^* = T_1. \end{aligned}\right\} \tag{6}$$

The following dimensionless quantities are introduced into Equations (1)–(6) (except 2),

$$y = \frac{y^*}{d}, \quad z = \frac{z^*}{d}, \quad t = t^*\omega^*, \quad u = \frac{u^*}{U_0}, \quad v = \frac{v^*}{V_0},$$
$$w = \frac{w^*}{V_0}, \quad \omega = \frac{\omega^* d^2}{\vartheta}, \quad p = \frac{p^*}{\rho_{hnf} V_0^2}, \quad \theta = \frac{T^* - T_1}{T_0 - T_1}.$$

The reduced equations take the form:

$$\frac{\partial v}{\partial y} + \frac{\partial w}{\partial z} = 0, \tag{7}$$

$$\frac{\omega}{Re}\frac{\partial v}{\partial t} + v\frac{\partial v}{\partial y} + w\frac{\partial v}{\partial z} = -\frac{\partial p}{\partial y} + \frac{1}{C_1 C_2 Re}\left(\frac{\partial^2 v}{\partial y^2} + \frac{\partial^2 v}{\partial z^2}\right), \tag{8}$$

$$\frac{\omega}{Re}\frac{\partial w}{\partial t} + v\frac{\partial w}{\partial y} + w\frac{\partial w}{\partial z} = -\frac{\partial p}{\partial z} + \frac{1}{C_1 C_2 Re}\left(\frac{\partial^2 w}{\partial y^2} + \frac{\partial^2 w}{\partial z^2}\right) - \frac{C_3}{C_2 Re}H^2 w, \tag{9}$$

$$\frac{\omega}{Re}\frac{\partial \theta}{\partial t} + v\frac{\partial \theta}{\partial y} + w\frac{\partial \theta}{\partial z} = \frac{C_6}{C_5 Pr Re}\left(\frac{\partial^2 \theta}{\partial y^2} + \frac{\partial^2 \theta}{\partial z^2}\right). \tag{10}$$

Equation (2) permutes to the following cases:
Case I: When the magnetic field is along the upward-moving plate (at $y = 0$)

$$\frac{\omega}{Re}\frac{\partial u}{\partial t} + v\frac{\partial u}{\partial y} + w\frac{\partial u}{\partial z} = \frac{1}{C_1 C_2 Re}\left(\frac{\partial^2 u}{\partial y^2} + \frac{\partial^2 u}{\partial z^2}\right) - \frac{C_3}{C_2 Re}H^2(u - 1) + C_4 Gr Re \theta. \tag{11}$$

Case II: When the magnetic field is along the downward-moving plate (at $y = 1$)

$$\frac{\omega}{Re}\frac{\partial u}{\partial t} + v\frac{\partial u}{\partial y} + w\frac{\partial u}{\partial z} = \frac{1}{C_1 C_2 Re}\left(\frac{\partial^2 u}{\partial y^2} + \frac{\partial^2 u}{\partial z^2}\right) - \frac{C_3}{C_2 Re}H^2(u + 1) + C_4 Gr Re \theta. \tag{12}$$

The reduced boundary conditions take the form:

$$\left.\begin{array}{c} y = 0, u = 1, v(z) = 1 + \varepsilon_1 \cos \pi z, w = 0, \theta = 1 + \varepsilon_2 e^{it}, \\ y = 1, u = -1, v = 1, w = 0, \theta = 0, \end{array}\right\} \tag{13}$$

where

$$Pr = \frac{(\mu c_p)_f}{k_f}, \quad Re = \frac{U_0 d}{\vartheta_f}, \quad H = B_0 d\sqrt{\frac{\sigma_f}{\rho_f \vartheta_f}}, \quad Gr = \frac{g\beta_f \vartheta_f (T_0 - T_1)}{U_0^3}$$

and the hybrid nanoliquid constants are explained in Table 1.

3 | METHOD OF SOLUTION

The reduced forms of the governing equations are resolved using the perturbation method. For this, let $\varepsilon = \min\{\varepsilon_1, \varepsilon_2\}$ be very small and suppose that solution is of the format

TABLE 1 Hybrid nanoliquid constants[1,2,29]

Effective dynamic viscosity	$C_1 = \frac{\mu_{hnf}}{\mu_f} = (1-\phi_1)^{2.5}(1-\phi_2)^{2.5}$
Effective density	$C_2 = \frac{\rho_{hnf}}{\rho_f} = (1-\phi_2)\left[1-\phi_1+\phi_1\left(\frac{\rho_{s1}}{\rho_f}\right)\right]+\phi_2\left(\frac{\rho_{s2}}{\rho_f}\right)$
Effective electrical conductivity	$C_3 = \frac{\sigma_{hnf}}{\sigma_f} = 1 + \frac{3\left(\frac{\phi_1\sigma_1+\phi_2\sigma_2}{\sigma_f}-(\phi_1+\phi_2)\right)}{2+\left(\frac{\phi_1\sigma_1+\phi_2\sigma_2}{(\phi_1+\phi_2)\sigma_f}\right)-\left(\frac{\phi_1\sigma_1+\phi_2\sigma_2}{\sigma_f}-(\phi_1+\phi_2)\right)}$
Effective coefficient of thermal expansion	$C_4 = \frac{\beta_{hnf}}{\beta_f} = (1-\phi_2)\left[1-\phi_1+\phi_1\left(\frac{\beta_{s1}}{\beta_f}\right)\right]+\phi_2\left(\frac{\beta_{s2}}{\beta_f}\right)$
Effective specific heat	$C_5 = \frac{(\rho C_p)_{hnf}}{(\rho C_p)_f} = (1-\phi_2)\left[1-\phi_1+\phi_1\left(\frac{(\rho c_p)_{s1}}{(\rho c_p)_f}\right)\right]+\phi_2\left(\frac{(\rho c_p)_{s2}}{(\rho c_p)_f}\right)$
Effective thermal conductivity	$C_6 = \frac{k_{hnf}}{k_f}$, where $\frac{k_{hnf}}{k_{nf}} = \frac{k_{s2}+2k_{nf}-2\phi_2(k_{nf}-k_{s2})}{k_{s2}+2k_{nf}+2\phi_2(k_{nf}-k_{s2})}$ and $\frac{k_{nf}}{k_f} = \frac{k_{s1}+2k_f-2\phi_1(k_f-k_{s1})}{k_{s1}+2k_f+2\phi_1(k_f-k_{s1})}$

$$f(y,z,t) = f_0(y) + \varepsilon f_1(y,z,t) + \varepsilon^2 f_2(y,z,t) + \ldots. \tag{14}$$

3.1 | Steady flow solution

Letting $\varepsilon = 0$, the current problem narrows to a steady 2D flow which is governed by the ensuing equations:

Case I: When the magnetic field is along the upward-moving plate (at $y = 0$)

$$u_0'' - C_1C_2Reu_0' - C_1C_3H^2(u_0-1) + C_1C_2C_4Re^2\,Gr\theta_0 = 0. \tag{15}$$

Case II: When the magnetic field is along the downward-moving plate (at $y = 1$)

$$u_0'' - C_1C_2Reu_0' - C_1C_3H^2(u_0+1) + C_1C_2C_4Re^2\,Gr\theta_0 = 0, \tag{16}$$

with $v_0 = 1, w_0 = 0, p_0 =$ constant and

$$\theta_0'' - \frac{C_5PrRe}{C_6}\theta_0' = 0, \tag{17}$$

where prime notates the derivative with respect to y.

The analogous boundary conditions take the form:

$$\left.\begin{aligned} y = 0, u_0 = 1, \theta_0 = 1,\\ y = 1, u_0 = -1, \theta_0 = 0.\end{aligned}\right\} \tag{18}$$

Solving Equations (15)–(17) with respect to (18) yields:

$$\theta_0 = \frac{1}{e^{a_1} - 1}(e^{a_1} - e^{a_1 y}). \tag{19}$$

Case I: When the magnetic field is along the upward-moving plate (at $y = 0$)

$$u_0 = \frac{1}{(e^{b_2} - e^{b_1})}\left(\left(\alpha_1 e^{b_2} - \beta_1\right)e^{b_1 y} + \left(\beta_1 - \alpha_1 e^{b_1}\right)e^{b_2 y}\right) + A_1 e^{a_1 y} + A_2 + 1. \tag{20}$$

Case II: When the magnetic field is along the downward-moving plate (at $y = 1$)

$$u_0 = \frac{1}{(e^{b_2} - e^{b_1})}\left(\left((\alpha_1 + 2)e^{b_2} - (\beta_1 + 2)\right)e^{b_1 y} + \left((\beta_1 + 2) - (\alpha_1 + 2)e^{b_1}\right)e^{b_2 y}\right) + A_1 e^{a_1 y} + A_2 - 1. \tag{21}$$

3.2 | Cross flow solution

Letting $\varepsilon \neq 0$, applying Equation (14) into Equations (7)–(9) and equating like powers of ε and ignoring the higher powers of ε^2, the following equations are derived:

$$\frac{\partial v_1}{\partial y} + \frac{\partial w_1}{\partial z} = 0, \tag{22}$$

$$\frac{\omega}{Re}\frac{\partial v_1}{\partial t} + \frac{\partial v_1}{\partial y} = -\frac{\partial p_1}{\partial y} + \frac{1}{C_1 C_2 Re}\left(\frac{\partial^2 v_1}{\partial y^2} + \frac{\partial^2 v_1}{\partial z^2}\right), \tag{23}$$

$$\frac{\omega}{Re}\frac{\partial w_1}{\partial t} + \frac{\partial w_1}{\partial y} = -\frac{\partial p_1}{\partial z} + \frac{1}{C_1 C_2 Re}\left(\frac{\partial^2 w_1}{\partial y^2} + \frac{\partial^2 w_1}{\partial z^2}\right) - \frac{C_3}{C_2 Re}H^2 w_1. \tag{24}$$

Corresponding boundary conditions are

$$\left.\begin{array}{r} y = 0, v_1 = \cos \pi z, w_1 = 0, \\ y = 1, v_1 = 0, w_1 = 0. \end{array}\right\} \tag{25}$$

These are the linear partial differential equations reporting the 3D cross flow, which is independent of the temperature field and the main flow component. The solutions for v_1, w_1, p_1 are assumed to be of the form:

$$v_1(y) = v_{11}(y)e^{it} + v_{12}(y)\cos \pi z, \tag{26}$$

$$w_1(y) = -(z v_{11}'(y)e^{it} + \frac{1}{\pi}v_{12}'(y)\sin \pi z), \tag{27}$$

$$p_1(y) = p_{11}(y)e^{it} + p_{12}(y)\cos \pi z, \tag{28}$$

where prime notates the derivative with respect to y. Expressions (26) and (27) have been chosen so that the equation of continuity (22) is trivially satisfied. Applying these into

Equations (23) and (24) and employing Equation (25), the solutions for v_1, w_1, p_1 are obtained as:

$$v_1 = \frac{1}{D}\sum_{i=1}^{4} D_i e^{r_i y}\cos \pi z, \tag{29}$$

$$w_1 = -\frac{1}{\pi D}\sum_{i=1}^{4} r_i D_i e^{r_i y}\sin \pi z, \tag{30}$$

$$p_1 = \frac{1}{C_1 C_2 Re \pi^2 D}\sum_{i=1}^{4} D_i\left(r_i^3 - C_1 C_2 Re r_i^2 - \left(C_1 C_3 H^2 + \pi^2\right) r_i\right) e^{r_i y}\cos \pi z. \tag{31}$$

3.3 | Temperature field

Comparably letting $\varepsilon \neq 0$, applying Equation (14) to Equation (10) and comparing like powers of ε, the equation for temperature field is given by:

$$\frac{\omega}{Re}\frac{\partial \theta_1}{\partial t} + \frac{\partial \theta_1}{\partial y} = \frac{C_6}{C_5 Pr Re}\left(\frac{\partial^2 \theta_1}{\partial y^2} + \frac{\partial^2 \theta_1}{\partial z^2}\right), \tag{32}$$

with

$$\left.\begin{aligned} y = 0, \theta_1 = e^{it}, \\ y = 1, \theta_1 = 0. \end{aligned}\right\} \tag{33}$$

Equation (32) along with Equation (33) is solved with a supposition that the solution is of the format:

$$\theta_1(y, z, t) = \theta_{11} e^{it} + \theta_{12}\cos \pi z. \tag{34}$$

Applying Equation (34) into (32), we obtain

$$\theta_{11}'' - \frac{C_5 Pr Re}{C_6}\theta_{11}' - \frac{C_5 Pr \omega i}{C_6}\theta_{11} = 0, \tag{35}$$

$$\theta_{12}'' - \frac{C_5 Pr Re}{C_6}\theta_{12}' - \pi^2 \theta_{12} = 0, \tag{36}$$

with

$$\left.\begin{aligned} y = 0, \theta_{11} = 1, \theta_{12} = 0, \\ y = 1, \theta_{11} = 0, \theta_{12} = 0. \end{aligned}\right\} \tag{37}$$

Resolving Equation (35) and (36) utilizing Equation (37), the solution is given by:

$$\theta_1(y, z, t) = \frac{1}{e^{a_3} - e^{a_2}}\left(e^{a_3} e^{a_2 y} - e^{a_2} e^{a_3 y}\right) e^{it}. \tag{38}$$

3.4 | Main flow solution

Letting $\varepsilon \neq 0$, the first-order equation for the main flow deduced with the help of Equation (14) and equating like powers of ε is given by:

$$\frac{\omega}{Re}\frac{\partial u_1}{\partial t} + \frac{\partial u_1}{\partial y} + v_1 u_0' = \frac{1}{C_1 C_2 Re}\left(\frac{\partial^2 u_1}{\partial y^2} + \frac{\partial^2 u_1}{\partial z^2}\right) - \frac{C_3}{C_2 Re} H^2 u_1 + C_4 GrRe\theta_1, \tag{39}$$

with

$$\left.\begin{array}{l} y = 0, u_1 = 0, \\ y = 1, u_1 = 0. \end{array}\right\} \tag{40}$$

Suppose the solution is of the format:

$$u_1(y, z, t) = u_{11}e^{it} + u_{12}\cos \pi z. \tag{41}$$

Applying Equation (41) in Equation (39) and comparing like powers of ε, we get:

$$u_{11}'' - C_1 C_2 Re u_{11}' - (C_1 C_2 \omega i + C_1 C_3 H^2)u_{11} = -C_1 C_2 C_4 Re^2\, Gr\theta_{11}, \tag{42}$$

$$u_{12}'' - C_1 C_2 Re u_{12}' - (\pi^2 + C_1 C_3 H^2)u_{12} = C_1 C_2 Re v_{12} u_0', \tag{43}$$

with

$$\left.\begin{array}{l} y = 0, u_{11} = 0, u_{12} = 0, \\ y = 1, u_{11} = 0, u_{12} = 0. \end{array}\right\} \tag{44}$$

Resolving Equation (42) and (43) utilizing Equation (44), the solution is derived as:
Case I: When the magnetic field is along the upward-moving plate (at $y = 0$)

$$\begin{aligned} u_1(y, z, t) = &\left\{\frac{1}{e^{b_4} - e^{b_3}}\left[\left(\alpha_2 e^{b_4} - \beta_2\right)e^{b_3 y} + \left(\beta_2 - \alpha_2 e^{b_3}\right)e^{b_4 y}\right] + A_3 e^{a_2 y} + A_4 e^{a_3 y}\right\}e^{it} \\ &+ \left\{\frac{1}{e^{b_6} - e^{b_5}}\left[\left(\alpha_3 e^{b_6} - \beta_3\right)e^{b_5 y} + \left(\beta_3 - \alpha_3 e^{b_5}\right)e^{b_6 y}\right]\right. \\ &\left.+ \sum_{i=1}^{4}\left[A_{i1}e^{(r_i + b_1)y} + A_{i2}e^{(r_i + b_2)y} + A_{i3}e^{(r_i + a_1)y}\right]\right\}\cos \pi z. \end{aligned} \tag{45}$$

Case II: When the magnetic field is along the downward-moving plate (at $y = 1$)

$$u_1(y,z,t) = \left\{\frac{1}{e^{b_4}-e^{b_3}}\left[\left(\alpha_2 e^{b_4}-\beta_2\right)e^{b_3 y}+\left(\beta_2-\alpha_2 e^{b_3}\right)e^{b_4 y}\right]+A_3 e^{a_2 y}+A_4 e^{a_3 y}\right\}e^{it}$$
$$+\left\{\frac{1}{e^{b_6}-e^{b_5}}\left[\left(\alpha_4 e^{b_6}-\beta_4\right)e^{b_5 y}+\left(\beta_4-\alpha_4 e^{b_5}\right)e^{b_6 y}\right]\right.$$
$$\left.+\sum_{i=1}^{4}\left[B_{i1}e^{(r_i+b_1)y}+B_{i2}e^{(r_i+b_2)y}+B_{i3}e^{(r_i+a_1)y}\right]\right\}\cos\pi z. \tag{46}$$

4 | DRAG COEFFICIENT AND HEAT TRANSFER RATE

Physical quantities like skin friction (Cf) and Nusselt number (Nu) measuring surface drag and rate of heat transfer, respectively, are given by:[24,28]

Case I: When the magnetic field is along the upward-moving plate (at $y = 0$)

$$Cf = \frac{d}{\mu_f U_0}\left|\mu_{hnf}\left(\frac{du^*}{dy^*}\right)_{y^*=d}\right| = \frac{1}{C_1}\left|\left(\frac{du_0}{dy}\right)_{y=1}+\varepsilon\left(\frac{du_1}{dy}\right)_{y=1}\right|. \tag{47}$$

Case II: When the magnetic field is along the downward-moving plate (at $y = 1$)

$$Cf = \frac{d}{\mu_f U_0}\left|\mu_{hnf}\left(\frac{du^*}{dy^*}\right)_{y^*=d}\right| = \frac{1}{C_1}\left|\left(\frac{du_0}{dy}\right)_{y=1}+\varepsilon\left(\frac{du_1}{dy}\right)_{y=1}\right|, \tag{48}$$

$$Nu = \frac{d}{k_f(T_0-T_1)}\left|k_{hnf}\left(\frac{dT^*}{dy^*}\right)_{y^*=d}\right| = C_6\left|\left(\frac{d\theta_0}{dy}\right)_{y=0}+\varepsilon\left(\frac{d\theta_1}{dy}\right)_{y=0}\right|. \tag{49}$$

5 | RESULT AND DISCUSSIONS

The significance of effectual parameters on velocity (u), surface drag (Cf), and temperature (θ) profiles are depicted through Figures 2–11. The physical properties of nanoparticles (Al_2O_3 and Fe_3O_4) and the conventional fluid (water) are identified in Table 2. $\phi_1 = 0.1, \phi_2 = 0.1, \omega = 10, Re = 1, H = 2, Pr = 7, Gr = 7,$ and $t = \pi/2$ are the base values of

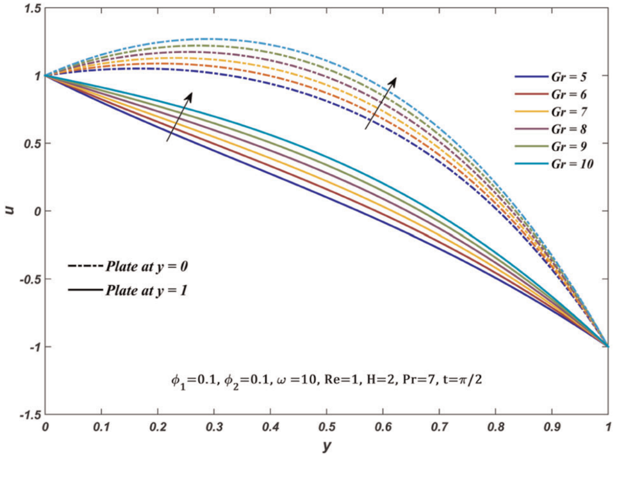

FIGURE 2 Deviation in u with Gr [Color figure can be viewed at wileyonlinelibrary.com]

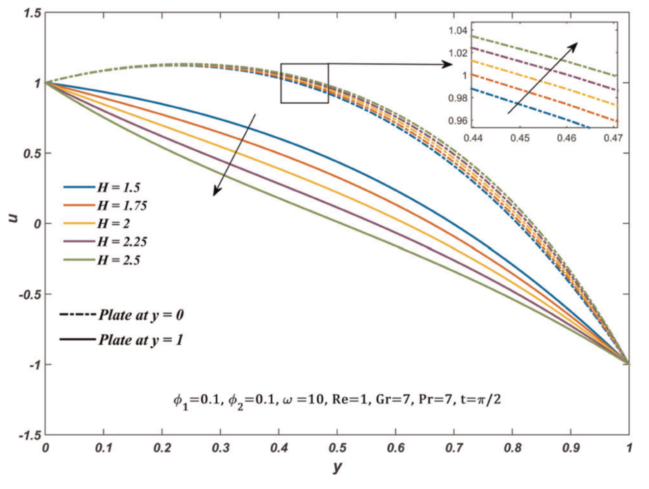

FIGURE 3 Deviation in u with H [Color figure can be viewed at wileyonlinelibrary.com]

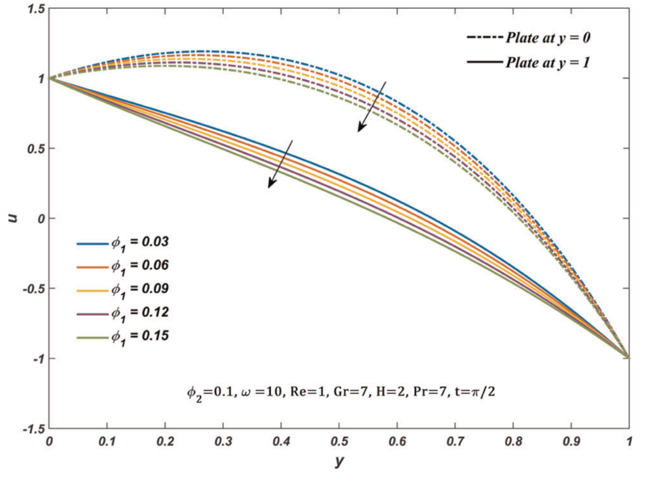

FIGURE 4 Deviation in u with ϕ_1 [Color figure can be viewed at wileyonlinelibrary.com]

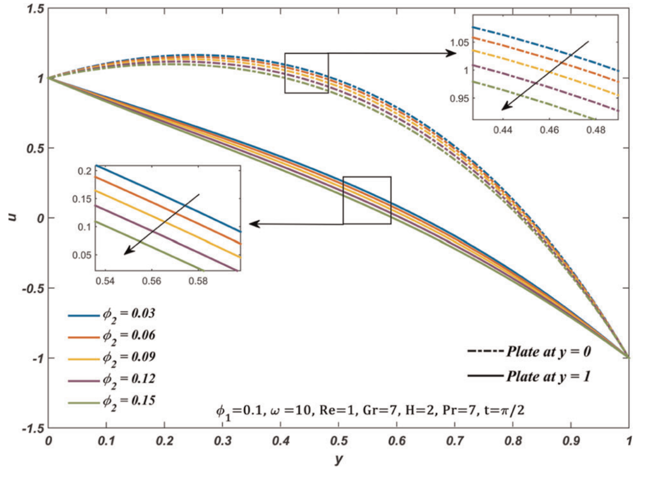

FIGURE 5 Deviation in u with ϕ_2 [Color figure can be viewed at wileyonlinelibrary.com]

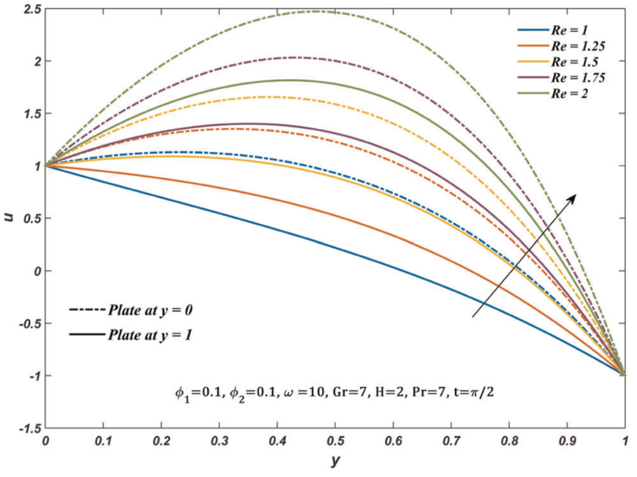

FIGURE 6 Deviation in u with Re [Color figure can be viewed at wileyonlinelibrary.com]

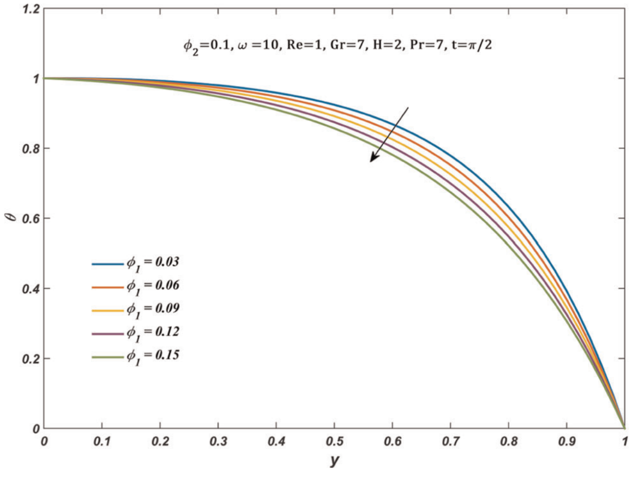

FIGURE 7 Deviation in θ with ϕ_1 [Color figure can be viewed at wileyonlinelibrary.com]

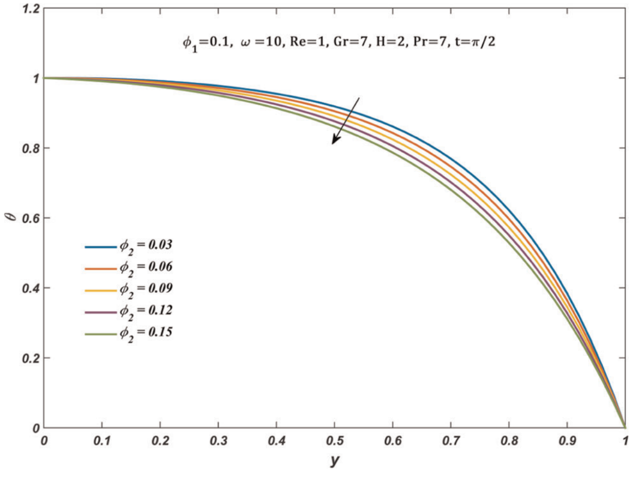

FIGURE 8 Deviation in θ with ϕ_2 [Color figure can be viewed at wileyonlinelibrary.com]

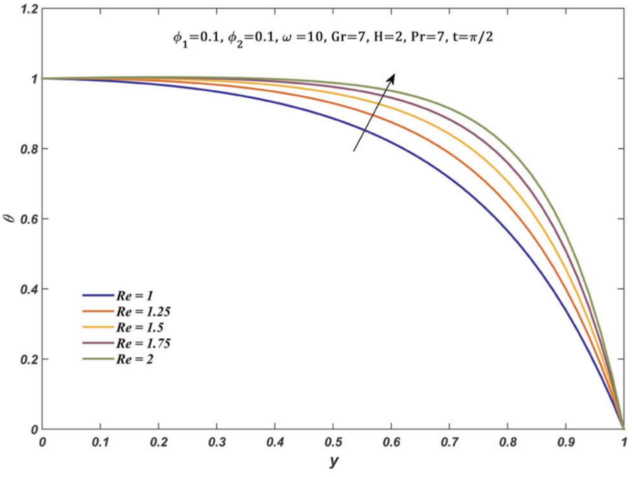

FIGURE 9 Deviation in θ with *Re* [Color figure can be viewed at wileyonlinelibrary.com]

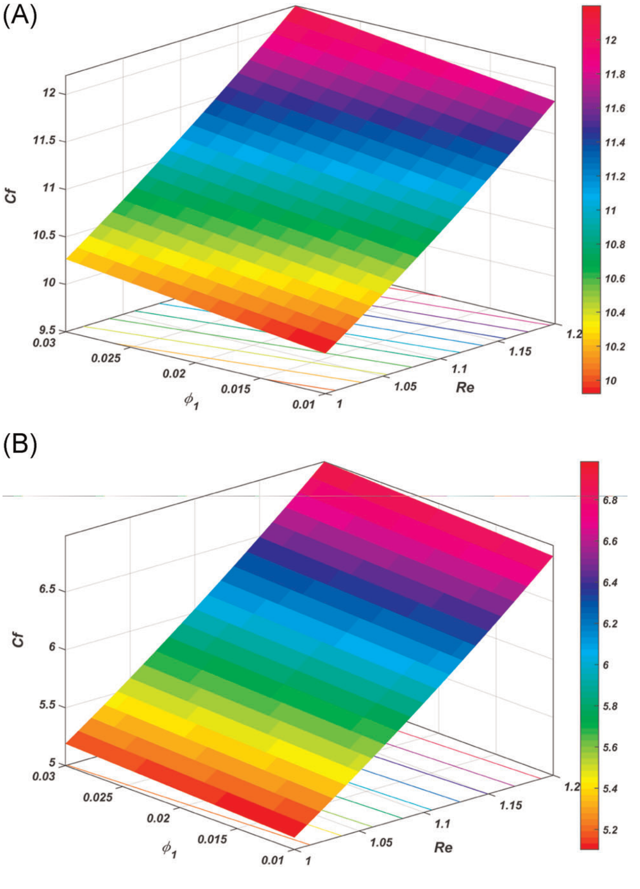

FIGURE 10 (A) Parallel deviation in *Cf* with ϕ_1 and *Re* on an upward-moving plate (at $y = 0$). (B) Parallel deviation in *Cf* with ϕ_1 and *Re* on a downward-moving plate (at $y = 1$) [Color figure can be viewed at wileyonlinelibrary.com]

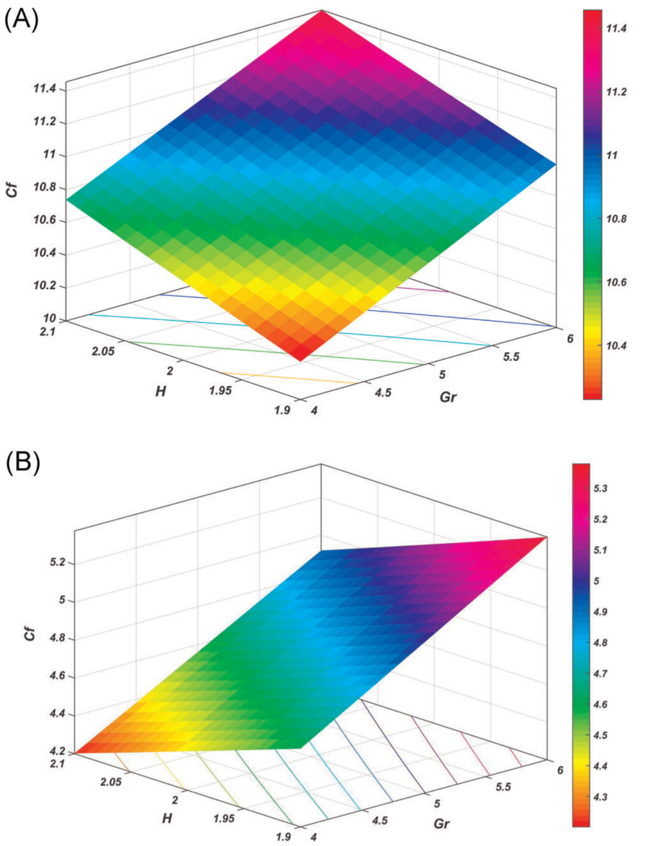

FIGURE 11 (A) Parallel deviation in Cf with H and Gr on an upward-moving plate (at $y = 0$). (B) Parallel deviation in Cf with H and Gr on a downward-moving plate (at $y = 1$) [Color figure can be viewed at wileyonlinelibrary.com]

TABLE 2 Physical properties of nanoparticles and base fluid[3,9,30]

Physical properties	H_2O	Al_2O_3	Fe_3O_4
ρ	997.1	3970	5180
C_p	4179	765	670
β	21×10^{-5}	0.85×10^{-5}	1.3×10^{-5}
σ	5×10^{-5}	35×10^{6}	25,000
k	0.613	40	9.7

parameters employed (unless specified) throughout the analysis. Furthermore, the validation of the obtained results is achieved through a comparative study with the work of Neethu et al.[28] (see Table 3) and a good agreement is noted.

Figure 2 explains the positive effect of Grashof number (Gr) on u meaning that an augmentation in Gr will increase the velocity. Physically, on magnifying Gr the buoyancy forces become prominent, which results in ascending the velocity profile. Figure 3 manifests the consequence of Hartmann number (H) on u. The introduction of a magnetic field produces a drag force (Lorentz force), which sets up an opposite reaction on upward- and downward-moving plates. On varying H, it is noted that u ascends on an upward-moving plate whereas u descends on a downward-moving plate. The negative influence of volume fraction of

TABLE 3 Comparison of *Nu* with augmenting *Re* values when $\phi_1 = 0, \phi_2 = 0, \omega = 10, t = \pi/2, Pr = 7, Gr = 5$, and $H = 2$

	Nu	
Re	**Neethu et al.**[28]	**Present study**
0.5	3.606813361	3.606813361
1	6.997602314	6.997602314
1.5	10.47713887	10.47713887
2	13.96647291	13.96647291
2.5	17.48348401	17.48348401

nanoparticles (ϕ_1 and ϕ_2) on u is elucidated in Figures 4 and 5, respectively. This decrease in velocity can be physically attributed to the fact that increasing volume fraction of nanoparticles swells the viscosity of hybrid nanoliquid, which causes a drop in velocity. The influence of the injection/suction parameter (Re) on u is depicted in Figure 6. Velocity profile experiences an exponential augmentation when Re values are improved.

Figures 7 and 8 reveal that intensification in the volume fraction of nanoparticles brings about a reduction in θ. The impact of Re on θ is displayed using Figure 9 and it is noted that Re causes an improvement in θ. Physically, this increase in temperature can be associated with the fact that with increasing Re values the heated nanoparticles enter the opposite moving plates and the cold nanoparticles exit the opposite moving plates.

The parallel effect of effectual parameters on drag coefficient (Cf) is illustrated in Figures 10 and 11 with the aid of 3D surface plots. The (A) and (B) parts of Figures 10 and 11 discuss the parallel effect on the upward- and downward-moving plate, respectively. From Figures 10 and 11, it is seen that surface drag ascends with ϕ_1, Re, H, and Gr on the upward-moving plate. Furthermore, surface drag ascends with ϕ_1, Re, and Gr and descends with H on the downward-moving plate.

6 | STATISTICAL ANALYSIS

6.1 | Response surface methodology

RSM is a statistical approach employed in analyzing the conjoint impact of effectual parameters (independent variables) on the physical quantity of interest (response/dependent variable). In

TABLE 4 Effective parameter levels

		Levels		
Parameter	**Symbol**	**−1 (low)**	**0 (medium)**	**1 (high)**
ϕ_1	A	0.02	0.05	0.08
ϕ_2	B	0.02	0.05	0.08
Re	C	1	1.5	2

TABLE 5 Experimental design with response

	Coded values			Actual values			Response
Run	***A***	***B***	***C***	ϕ_1	ϕ_2	***Re***	***Nu***
1	−1	−1	−1	0.02	0.02	1	6.9437
2	1	−1	−1	0.08	0.02	1	6.8562
3	−1	1	−1	0.02	0.08	1	6.895
4	1	1	−1	0.08	0.08	1	6.8352
5	−1	−1	1	0.02	0.02	2	13.8524
6	1	−1	1	0.08	0.02	2	13.6411
7	−1	1	1	0.02	0.08	2	13.7266
8	1	1	1	0.08	0.08	2	13.53
9	−1	0	0	0.02	0.05	1.5	10.3412
10	1	0	0	0.08	0.05	1.5	10.19
11	0	−1	0	0.05	0.02	1.5	10.309
12	0	1	0	0.05	0.08	1.5	10.2216
13	0	0	−1	0.05	0.05	1	6.8773
14	0	0	1	0.05	0.05	2	13.6873
15	0	0	0	0.05	0.05	1.5	10.2646
16	0	0	0	0.05	0.05	1.5	10.2646
17	0	0	0	0.05	0.05	1.5	10.2646
18	0	0	0	0.05	0.05	1.5	10.2646
19	0	0	0	0.05	0.05	1.5	10.2646
20	0	0	0	0.05	0.05	1.5	10.2646

this problem, *Nu* is chosen as the response variable and nanoparticle volume fraction of $Al_2O_3 (0.02 \le \phi_1 \le 0.08)$, the nanoparticle volume fraction of $Fe_3O_4 (0.02 \le \phi_2 \le 0.08)$ and injection/suction parameter $(1 \le Re \le 2)$ are chosen as the influential parameters. Table 4 bespeaks the effective parameters and their levels. The general model (adopting central composite design) for response variable involving linear, interactive, and quadratic terms is expressed by:

$$\text{Response} = \lambda_0 + \lambda_1 A + \lambda_2 B + \lambda_3 C + \lambda_4 AB + \lambda_5 BC + \lambda_6 AC + +\lambda_7 A^2 + \lambda_8 B^2 + \lambda_9 C^2, \tag{50}$$

where $\lambda_i (i = 0,1, \ldots, 9)$ represents the regression coefficients. The experimental design and the response for the 20 runs (according to CCD) are given in Table 5.

The analysis of variable table (Table 6) illustrates the efficiency of the estimated model. A parameter is claimed as significant if the corresponding F value is greater than 1 and the corresponding p value is less than .05. It is observed that the quadratic terms in ϕ_1 and ϕ_2 are not significant. Hence, these terms are removed from the model. The coefficient of determination (R^2) for the model is found to be 100% which boosts the model accuracy.

TABLE 6 Analysis of variable table

	Degree of freedom	Adjusted sum of squares	Adjusted mean squares	Regression coefficient	F value	p Value
Model	9	115.884	12.876		924,250.49	.000
Linear	3	115.870	38.623		2,772,413.38	.000
ϕ_1	1	0.050	0.050	−0.07064	3581.88	.000
ϕ_2	1	0.016	0.016	−0.03940	1114.30	.000
Re	1	115.804	115.804	3.40300	8,312,543.94	.000
Square	3	0.002	0.001		46.00	.000
$\phi_1 \times \phi_1$	1	0.000	0.000	0.00137	0.37	**.556**
$\phi_2 \times \phi_2$	1	0.000	0.000	0.00107	0.23	**.644**
$Re \times Re$	1	0.001	0.001	0.01807	64.47	.000
Two-way interaction	3	0.012	0.004		292.11	.000
$\phi_1 \times \phi_2$	1	0.000	0.000	0.00530	16.13	.002
$\phi_1 \times Re$	1	0.008	0.008	−0.03258	609.35	.000
$\phi_2 \times Re$	1	0.003	0.003	−0.02090	250.84	.000
Constant				10.2645		
Error	10	0.000	0.000			
Lack-of-fit	5	0.000	0.000		*	*
Pure error	5	0.000	0.000			
Total	19	115.884				
	$R^2 = 100\%$			Adjusted $R^2 = 100\%$		

The fitted quadratic model for Nu is given by:

$$\begin{aligned} Nu = {} & 10.2645 - 0.07064\phi_1 - 0.0394\phi_2 + 3.403Re + 0.01807Re^2 + 0.0053\phi_1\phi_2 \\ & - 0.03258\phi_1 Re - 0.0209\phi_2 Re. \end{aligned} \tag{51}$$

The reliability of the estimated model for Nu is further clarified using residual plots (see Figure 12). All points in a normal probability plot situated beside a straight line with an insignificant deflection and the residual histogram are approximately bell-shaped confirming the normal nature of residuals. Furthermore, a maximum error of 0.005 can be observed from the fitted versus residual plot, which also contributes to the accuracy of the model.

From Equation (51), it can be inferred that ϕ_1 *and* ϕ_2 have a negative impact on Nu and Re has a positive effect on Nu. The parallel interaction of two parameters on Nu is graphed using surface and contour plots (see Figure 13) by fixing the third parameter at the medium level. From Figure 13A–C, it is perceived that Nu is highest for smaller values of ϕ_1 *and* ϕ_2 and larger values of Re.

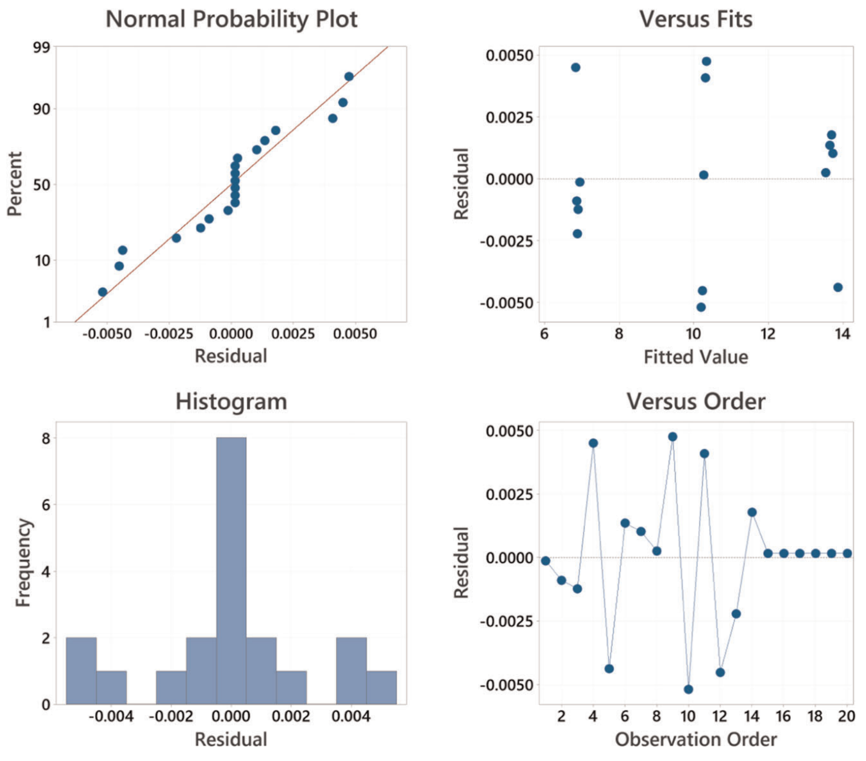

FIGURE 12 Residual plots [Color figure can be viewed at wileyonlinelibrary.com]

6.2 | Sensitivity analysis

Sensitivity analysis is a statistical technique that measures the extent and nature of dependency exhibited by the effectual parameters on the physical quantity of interest. In other words, sensitivity analysis accounts for the variation induced by the augmenting parameter on the remaining effectual parameter. The sign of sensitivity (positive or negative) signifies the nature of the correlation between Nu and the influential parameters. Furthermore, the magnitude of sensitivity indicates the intensity of the effect on Nu.

The quadratic model (in coded form) after neglecting the insignificant terms is given by:

$$Nu = 10.2645 - 0.07064A - 0.0394B + 3.403C + 0.01807C^2 + 0.0053AB - 0.03258AC - 0.0209BC. \tag{52}$$

Then the sensitivity functions are:

$$\frac{\partial Nu}{\partial A} = -0.07064 + 0.0053B - 0.03258C, \tag{53}$$

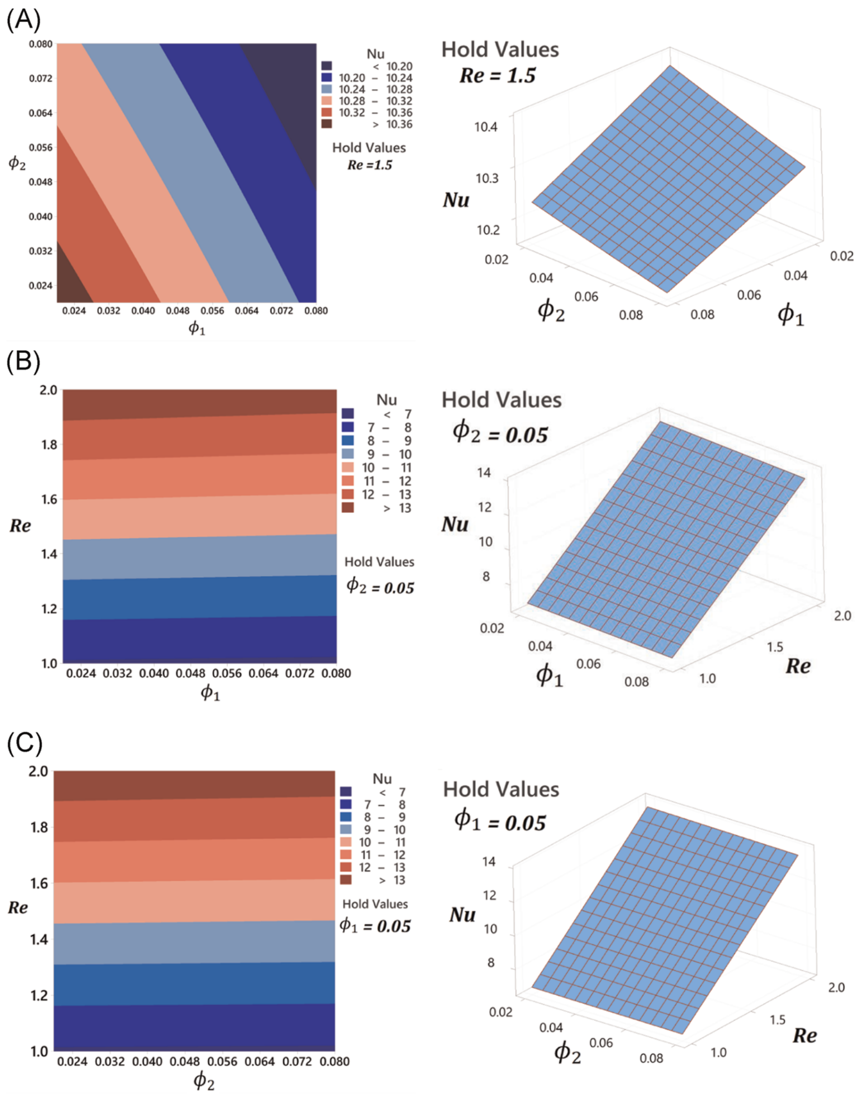

FIGURE 13 Contour and surface plots for *Nu* [Color figure can be viewed at wileyonlinelibrary.com]

$$\frac{\partial Nu}{\partial B} = -0.0394 + 0.0053A - 0.0209C, \tag{54}$$

$$\frac{\partial Nu}{\partial C} = 3.403 + 0.03614C - 0.03258A - 0.0209B. \tag{55}$$

The sensitivity for *Nu* is tabulated in Table 7 keeping ϕ_1 in the medium level. It is noted that ϕ_1 and ϕ_2 exhibits negative sensitivity and *Re* exhibits a positive sensitivity toward *Nu*. The sensitivity of *Nu* is also visualized using bar charts (Figure 14). It is seen that the results of sensitivity analysis are in perfect harmony with the results inferred using RSM. It is also noticed that *Nu* is most sensitive with *Re*.

TABLE 7 Sensitivity of response Nu when $A = 0$

B	C	Sensitivity $\frac{\partial Nu}{\partial A}$	$\frac{\partial Nu}{\partial B}$	$\frac{\partial Nu}{\partial C}$
−1	−1	−0.0434	−0.0185	3.3878
	0	−0.0759	−0.0394	3.4239
	1	−0.1085	−0.0603	3.4600
0	−1	−0.0381	−0.0185	3.3669
	0	−0.0706	−0.0394	3.4030
	1	−0.1032	−0.0603	3.4391
1	−1	−0.0328	−0.0185	3.3460
	0	−0.0653	−0.0394	3.3821
	1	−0.0979	−0.0603	3.4182

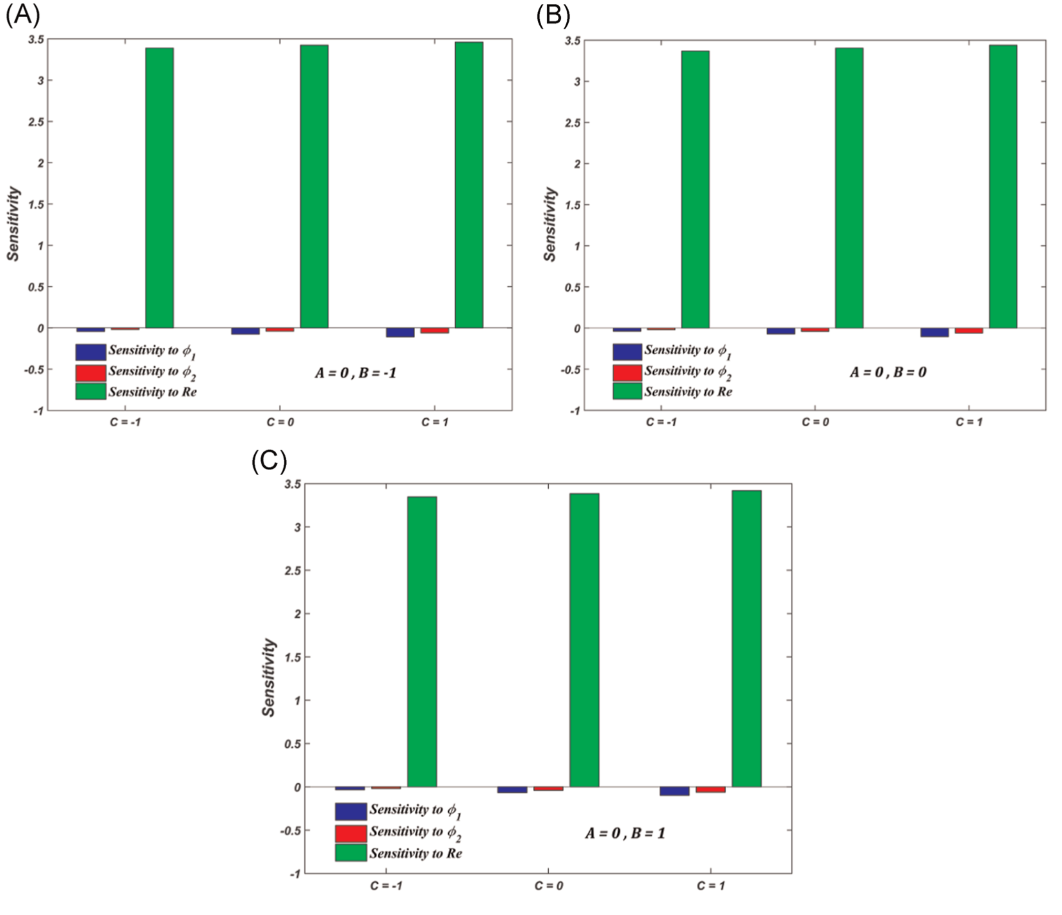

FIGURE 14 Bar charts depicting the sensitivity of Nu [Color figure can be viewed at wileyonlinelibrary.com]

7 | CONCLUDING REMARKS

The key observations are:

- Grashof number has a constructive effect on main flow velocity.
- Hartman number positively contributes toward the velocity profile on the upward-moving plate and negatively contributes toward the velocity profile on the downward-moving plate.
- The main flow velocity profile is higher when a magnetic field is applied on the upward-moving plate.
- The drag coefficient is directly proportional to the volume fraction of nanoparticles.
- The rate of heat transfer is the most sensitive parameter with the injection/suction parameter.
- Augmentation of volume fraction of Al_2O_3 nanoparticles has more influence on the flow profiles.
- The surface drag coefficient ascends with augmenting the Hartmann number on the upward-moving plate and descends on the downward-moving plate.
- The volume fraction of nanoparticles exhibits a destructive effect on the heat transfer rate.

NOMENCLATURE

u^*, v^*, w^*	velocity components, m/s
T^*	fluid temperature, K
t^*	time, s
T_0	temperature of the fluid near the plate at origin, K
T_1	temperature of the fluid near the plate at d, K
g	acceleration due to gravity, m/s^2
U_0	velocity of the moving plates
p^*	pressure
C_p	specific heat at constant pressure
B_0	strength of magnetic field
Re	injection/suction parameter
Pr	Prandtl number
H	Hartmann number
Gr	Grashof number
V_0	injection velocity

GREEK SYMBOLS

σ	electrical conductivity
ϕ_1, ϕ_2	nanoparticle volume fraction
k	thermal conductivity, W/m·K
ϑ	kinematic viscosity, m^2/s
μ	dynamic viscosity, kg/m·s
ω^*	angular velocity
ρ	density, kg/m^3
$\varepsilon_0, \varepsilon_1, \varepsilon_2$	very small reference constants

SUBSCRIPTS

f	base fluid
nf	nanoliquid
hnf	hybrid nanoliquid

s_1 Al_2O_3 nanoparticle
s_2 Fe_3O_4 nanoparticle

DATA AVAILABILITY STATEMENT

Data sharing is not applicable to this article as no new data were created or analyzed in this study.

ORCID

Alphonsa Mathew https://orcid.org/0000-0002-3810-4484
Sujesh Areekara https://orcid.org/0000-0001-7860-8268

REFERENCES

1. Junoh MM, Ali FM, Arifin NM, Bachok N, Pop I. MHD stagnation-point flow and heat transfer past a stretching/shrinking sheet in a hybrid nanofluid with induced magnetic field. *Int J Numer Methods Heat Fluid Flow*. 2019;30:1345-1364. https://doi.org/10.1108/HFF-06-2019-0500
2. Acharya N, Mabood F. On the hydrothermal features of radiative Fe_3O_4–graphene hybrid nanofluid flow over a slippery bended surface with heat source/sink. *J Therm Anal Calorim*. 2021;143:1273-1289. https://doi.org/10.1007/s10973-020-09850-1
3. Rostami MN, Dinarvand S, Pop I. Dual solutions for mixed convective stagnation-point flow of an aqueous silica–alumina hybrid nanofluid. *Chin J Phys*. 2018;56:2465-2478. https://doi.org/10.1016/j.cjph.2018.06.013
4. Aly EH, Pop I. Merkin and Needham wall jet problem for hybrid nanofluids with thermal energy. *Eur J Mech B/Fluids*. 2020;83:195-204. https://doi.org/10.1016/j.euromechflu.2020.05.004
5. Ghalambaz M, Roşca NC, Roşca AV, Pop I. Mixed convection and stability analysis of stagnation-point boundary layer flow and heat transfer of hybrid nanofluids over a vertical plate. *Int J Numer Methods Heat Fluid Flow*. 2019;30:3737-3754. https://doi.org/10.1108/HFF-08-2019-0661
6. Tayebi T, Chamkha AJ. Entropy generation analysis due to MHD natural convection flow in a cavity occupied with hybrid nanofluid and equipped with a conducting hollow cylinder. *J Therm Anal Calorim*. 2020;139:2165-2179. https://doi.org/10.1007/s10973-019-08651-5
7. Jha BK, Aina B. Role of induced magnetic field on MHD natural convection flow in vertical microchannel formed by two electrically non-conducting infinite vertical parallel plates. *Alex Eng J*. 2016;55:2087-2097. https://doi.org/10.1016/j.aej.2016.06.030
8. Dash GC, Ojha KL. Viscoelastic hydromagnetic flow between two porous parallel plates in the presence of sinusoidal pressure gradient. *Alex Eng J*. 2018;57:3463-3471. https://doi.org/10.1016/j.aej.2017.12.011
9. Sabu AS, Mathew A, Neethu TS, Anil George K. Statistical analysis of MHD convective ferro-nanofluid flow through an inclined channel with hall current, heat source and soret effect. *Therm Sci Eng Prog*. 2021;22:100816. https://doi.org/10.1016/j.tsep.2020.100816
10. Nandi S, Kumbhakar B. Unsteady MHD free convective flow past a permeable vertical plate with periodic movement and slippage in the presence of Hall current and rotation. *Therm Sci Eng Prog*. 2020;19:100561. https://doi.org/10.1016/j.tsep.2020.100561
11. Sabu AS, Areekara S, Mathew A. Statistical analysis on three-dimensional MHD convective Carreau nanofluid flow due to bilateral nonlinear stretching sheet with heat source and zero mass flux condition. *Heat Transfer*. 2021;50(4):3641-3660. https://doi.org/10.1002/htj.22045
12. Ali L, Tassaddiq A, Ali R, et al. A new analytical approach for the research of thin-film flow of magneto hydrodynamic fluid in the presence of thermal conductivity and variable viscosity. *Z Angew Math Mech*. 2021;101:e201900292. https://doi.org/10.1002/zamm.201900292
13. Nayak MK, Akbar NS, Tripathi D, Pandey VS. Three dimensional MHD flow of nanofluid over an exponential porous stretching sheet with convective boundary conditions. *Therm Sci Eng Prog*. 2017;3:133-140. https://doi.org/10.1016/j.tsep.2017.07.006
14. Das S, Tarafdar B, Jana RN. Hall effects on unsteady MHD rotating flow past a periodically accelerated porous plate with slippage. *Eur J Mech B/Fluids*. 2018;72:135-143. https://doi.org/10.1016/j.euromechflu.2018.04.010

15. Ahmed S, Zueco J, López-González LM. Numerical and analytical solutions for magneto-hydrodynamic 3D flow through two parallel porous plates. *Int J Heat Mass Transfer*. 2017;108:322-331. https://doi.org/10.1016/j.ijheatmasstransfer.2016.11.102
16. Krishna MV, Chamkha AJ. Hall and ion slip effects on MHD rotating flow of elastico-viscous fluid through porous medium. *Int Commun Heat Mass Transfer*. 2020;113:104494. https://doi.org/10.1016/j.icheatmasstransfer.2020.104494
17. Noreen S, Quratulain, Tripathi D. Heat transfer analysis on electroosmotic flow via peristaltic pumping in non-Darcy porous medium. *Therm Sci Eng Prog*. 2019;11:254-262. https://doi.org/10.1016/j.tsep.2019.03.015
18. Maskaniyan M, Nazari M, Rashidi S, Mahian O. Natural convection and entropy generation analysis inside a channel with a porous plate mounted as a cooling system. *Therm Sci Eng Prog*. 2018;6:186-193. https://doi.org/10.1016/j.tsep.2018.04.003
19. Krishna MV, Chamkha AJ. Hall and ion slip effects on MHD rotating boundary layer flow of nanofluid past an infinite vertical plate embedded in a porous medium. *Results Phys*. 2019;15:102652. https://doi.org/10.1016/j.rinp.2019.102652
20. Mahanthesh B, Mackolil J. Flow of nanoliquid past a vertical plate with novel quadratic thermal radiation and quadratic Boussinesq approximation: sensitivity analysis. *Int Commun Heat Mass Transfer*. 2021;120:105040. https://doi.org/10.1016/j.icheatmasstransfer.2020.105040
21. Mahanthesh B, Thriveni K. Sensitivity analysis of heat transfer in nanoliquid with inclined magnetic field, exponential space-based heat source, convective heating, and slip effects. *Heat Transfer*. 2021;50(3):2362-2379. https://doi.org/10.1002/htj.21982
22. Abdelmalek Z, Mahanthesh B, Basir F, et al. Mixed radiated magneto Casson fluid flow with Arrhenius activation energy and Newtonian heating effects: flow and sensitivity analysis. *Alex Eng J*. 2020;59:3991-4011. https://doi.org/10.1016/j.aej.2020.07.006
23. Reddy ES, Panda S, Nayak MK, Makinde OD. Cross flow on transient double-diffusive natural convection in inclined porous trapezoidal enclosures. *Heat Transfer*. 2021;50:849-875. https://doi.org/10.1002/htj.21908
24. Singh K, Mathew A. Three dimensional MHD fluctuating free convective flow between two vertical porous plates moving in opposite directions. *J Rajasthan Acad Phys Sci*. 2009;8:457-474.
25. Gupta U, Jha AK, Chaudhary RC. Free convection flow between vertical plates moving in opposite direction and partially filled with porous medium. *Appl Math*. 2011;02:935-941. https://doi.org/10.4236/am.2011.28128
26. Gupta VG, Jain A, Jha AK. Convective effects on MHD flow and heat transfer between vertical plates moving in opposite direction and partially filled with a porous medium. *J Appl Math Phys*. 2016;4:341-358. https://doi.org/10.4236/jamp.2016.42041
27. Singh K, Mathew A. Heat transfer in three dimensional MHD flow between two parallel porous plates moving in opposite directions with transpiration cooling. *Proc Natl Acad Sci India A*. 2009;79:291-302.
28. Neethu TS, Areekara S, Mathew A. Statistical approach on 3D hydromagnetic flow of water-based nanofluid between two vertical porous plates moving in opposite directions. *Heat Transfer*. 2021. https://doi.org/10.1002/htj.22120
29. Manjunatha S, Kuttan BA, Jayanthi S, Chamkha A, Gireesha BJ. Heat transfer enhancement in the boundary layer flow of hybrid nanofluids due to variable viscosity and natural convection. *Heliyon*. 2019;5:e01469. https://doi.org/10.1016/j.heliyon.2019.e01469
30. Mackolil J, Mahanthesh B. Heat transfer enhancement using temperature-dependent effective properties of alumina-water nanoliquid with thermo-solutal Marangoni convection: a sensitivity analysis. *Appl Nanosci*. 2021. https://doi.org/10.1007/s13204-020-01631-4

How to cite this article: Mathew A, Neethu TS, Areekara S. Three-dimensional hydromagnetic hybrid nanoliquid flow and heat transfer between two vertical porous plates moving in opposite directions: Sensitivity analysis. *Heat Transfer*. 2021;1-24. https://doi.org/10.1002/htj.22192

APPENDIX

$$a_1 = \frac{C_5 PrRe}{C_6} \qquad \alpha_1 = -(A_1 + A_2)$$

$$b_1 = \frac{C_1C_2Re + \sqrt{C_1^2C_2^2Re^2 + 4C_1C_3H^2}}{2} \qquad \beta_1 = -(2 + A_1e^{a_1} + A_2)$$

$$b_2 = \frac{C_1C_2Re - \sqrt{C_1^2C_2^2Re^2 + 4C_1C_3H^2}}{2} \qquad b_3 = \frac{C_1C_2Re + \sqrt{C_1^2C_2^2Re^2 + 4\left(i\omega C_1C_2 + C_1C_3H^2\right)}}{2}$$

$$A_1 = \frac{C_1C_2C_4Re^2\,Gr}{(e^{a_1}-1)(a_1{}^2 - C_1C_2Rea_1 - C_1C_3H^2)} \qquad b_4 = \frac{C_1C_2Re - \sqrt{C_1^2C_2^2Re^2 + 4\left(i\omega C_1C_2 + C_1C_3H^2\right)}}{2}$$

$$A_2 = \frac{C_1C_2C_4Re^2\,Gre^{a_1}}{(e^{a_1}-1)C_1C_3H^2} \qquad D = D_1 + D_2 + D_3 + D_4$$

$$D_1 = r_3r_4(e^{r_2+r_4} - e^{r_2+r_3}) + r_2r_4(e^{r_3+r_2} - e^{r_3+r_4}) + r_2r_3(e^{r_3+r_4} - e^{r_2+r_4})$$

$$D_2 = r_3r_4(e^{r_1+r_3} - e^{r_1+r_4}) + r_1r_4(e^{r_3+r_4} - e^{r_3+r_1}) + r_1r_3(e^{r_1+r_4} - e^{r_3+r_4})$$

$$D_3 = r_2r_4(e^{r_1+r_4} - e^{r_1+r_2}) + r_1r_4(e^{r_2+r_1} - e^{r_2+r_4}) + r_1r_2(e^{r_2+r_4} - e^{r_1+r_4})$$

$$D_4 = r_2r_3(e^{r_1+r_2} - e^{r_1+r_3}) + r_1r_3(e^{r_3+r_2} - e^{r_2+r_1}) + r_1r_2(e^{r_1+r_3} - e^{r_2+r_3})$$

$$a_2 = \frac{\frac{C_5PrRe}{C_6} + \sqrt{\frac{C_5^2Pr^2Re^2}{C_6^2} + \frac{4C_5Pr\omega i}{C_6}}}{2} \qquad a_3 = \frac{\frac{C_5PrRe}{C_6} - \sqrt{\frac{C_5^2Pr^2Re^2}{C_6^2} + \frac{4C_5Pr\omega i}{C_6}}}{2}$$

$$A_3 = \frac{C_1C_2C_4Re^2\,Gre^{a_3}}{\left(e^{a_2} - e^{a_3}\right)\left(a_2^2 - C_1C_2Rea_2 - C_1C_2i\omega - C_1C_3H^2\right)}$$

$$A_4 = \frac{C_1C_2C_4Re^2\,Gre^{a_2}}{\left(e^{a_3} - e^{a_2}\right)\left(a_3^2 - C_1C_2Rea_3 - C_1C_2i\omega - C_1C_3H^2\right)}$$

$$\alpha_2 = -(A_3 + A_4) \qquad b_5 = \frac{C_1C_2Re + \sqrt{C_1^2C_2^2Re^2 + 4\left(C_1C_3H^2 + \pi^2\right)}}{2}$$

$$\beta_2 = -(A_3e^{a_2} + A_4e^{a_3}) \qquad b_6 = \frac{C_1C_2Re - \sqrt{C_1^2C_2^2Re^2 + 4\left(C_1C_3H^2 + \pi^2\right)}}{2}$$

$$A_{i1} = \frac{b_1(\alpha_1e^{b_2} - \beta_1)C_1C_2ReD_i}{\left(e^{b_2} - e^{b_1}\right)D\left[(r_i + b_1)^2 - C_1C_2Re(r_i + b_1) - (C_1C_3H^2 + \pi^2)\right]},\ i = 1,2,3,4$$

$$A_{i2} = \frac{b_2(\beta_1 - \alpha_1e^{b_1})C_1C_2ReD_i}{(e^{b_2} - e^{b_1})\,D\,\left[(r_i + b_2)^2 - C_1C_2Re(r_i + b_2) - (C_1C_3H^2 + \pi^2)\right]},\ i = 1,2,3,4$$

$$B_{i1} = \frac{b_1((\alpha_1 + 2)\,e^{b_2} - (\beta_1 + 2))C_1C_2ReD_i}{\left(e^{b_2} - e^{b_1}\right)D\left[\left(r_i + b_1\right)^2 - C_1C_2Re\left(r_i + b_1\right) - \left(C_1C_3H^2 + \pi^2\right)\right]},\ i = 1,2,3,4$$

$$B_{i2} = \frac{b_2((\beta_1 + 2) - (\alpha_1 + 2)e^{b_1})C_1C_2ReD_i}{(e^{b_2} - e^{b_1})\,D\,\left[(r_i + b_2)^2 - C_1C_2Re(r_i + b_2) - (C_1C_3H^2 + \pi^2)\right]},\ i = 1,2,3,4$$

$$B_{i3} = A_{i3} = \frac{a_1A_1C_1C_2ReD_i}{D\left[\left(r_i + a_1\right)^2 - C_1C_2Re(r_i + a_1) - (C_1C_3H^2 + \pi^2)\right]},\ i = 1,2,3,4$$

$$\alpha_3 = -\sum_{i=1}^{4}(A_{i1} + A_{i2} + A_{i3}) \qquad \alpha_4 = -\sum_{i=1}^{4}(B_{i1} + B_{i2} + B_{i3})$$

$$\beta_3 = -\sum_{i=1}^{4}\left(A_{i1}e^{(r_i+b_1)} + A_{i2}e^{(r_i+b_2)} + A_{i3}e^{(r_i+a_1)}\right)$$

$$\beta_4 = -\sum_{i=1}^{4}\left(B_{i1}e^{(r_i+b_1)} + B_{i2}e^{(r_i+b_2)} + B_{i3}e^{(r_i+a_1)}\right)$$